Journal of Power Sources 195 (2010) 1383–1392

Contents lists available at ScienceDirect

Journal of Power Sources

journal homepage: www.elsevier.com/locate/jpowsour

A high efficient assembly technique for large proton exchange membrane fuel cell stacks: Part II. Applications

P. Lin, P. Zhou, C.W. Wu*

State Key Lab of Structural Analysis for Industrial Equipment, Faculty of Vehicle Engineering and Mechanics, Dalian University of Technology, Dalian, Liaoning 116024, China

ARTICLE INFO

Article history:
Received 15 September 2009
Accepted 15 September 2009
Available online 28 September 2009

Keywords:
Fuel cell
Proton exchange membrane
Clamping load
Assembly technique

ABSTRACT

A high efficient assembly technique for large proton exchange membrane fuel cell (PEMFC) stacks is proposed for obtaining the optimal clamping load. Using the equivalent stiffness model proposed in Part I of this study, we show how to design the structure components for a large PEMFC stack. First, we give a design demonstration based on the structural strength of the stack. We then discuss how to obtain the optimal clamping load for a given PEMFC stack according to the requirements of the interface contact resistance and permeability of the gas diffusion layer. Finally, we discuss the effects of the equivalent stiffness of the spring washer on the structure thermal stress.

© 2009 Elsevier B.V. All rights reserved.

1. Introduction

Proton exchange membrane fuel cells (PEMFCs) have many advantages such as their clean and quiet operation, high efficiency, low operation temperature, and quick start-up, and they are therefore a possible alternative to combustion engines. Studies on a single PEMFC during the past decade have given a very good understanding of its basic principles. However, in the last few years, the performance of a large PEMFC stack has attracted more and more attention. To design a fuel cell stack with high reliability and long lifetime, there are a number of new technologies that need to be developed. Among them, the assembly is known to be a key technique, with previous studies having shown that the clamping load (clamping pressure) of a single PEMFC plays an important role in optimizing its performance [1–7]. In Part I of this study [8], a high efficient assembly model was proposed, where a large PEMFC stack system was considered as a mechanical equivalent stiffness model consisting of numerous elastic elements (springs) connected in either series or parallel. Comparison with a three-dimensional (3D) finite element analysis (FEA) showed that the equivalent stiffness model had very good prediction accuracy for calculating the component stiffness and clamping load. In the present paper, practical examples are introduced to show how to design the optimal clamping load for a large PEMFC stack using the equivalent stiffness model. However, the basic idea can be used in designing other types of fuel cells as well.

The clamping load of a large PEMFC stack affects the performance and lifetime in several ways. Too large a clamping load may cause some components in the stack to produce a stress high enough to give rise to plastic deformation or even crack [9], while too small a clamping load may result in a high contact electrical resistance at the interface between the gas diffusion layer (GDL) and the bipolar plate (BPP) [1–3] or the leakage of water or fuel at the sealed interfaces [10]. Even if a reasonable initial clamping load is applied at room temperature, either the contact electrical resistance or the sealed interface pressure or the structural stress may fail to meet the design criteria when considering the thermal effects under working conditions. Therefore, the thermal effects should be taken into consideration when calculating the pressure distribution inside PEMFC stacks. However, the computing time for such a large stack using a numerical method (usually FEA) is usually unacceptable owing to the complexity of the stack structure. In the past, a few attempts have been made to simulate the compression pressure within a single PEMFC [4,11–13]. Even for a single cell computational model, it usually takes a few hours for a step computation. In the following, we give a detailed description of how to obtain solutions for the problems mentioned above using the spring assembly model proposed in the previous study [8].

2. Pretension and tightening torque of clamping bolts

In the traditional PEMFC stacks, end plates (EPs) together with an array of bolts are usually used to fasten the inner components, as shown in Fig. 1. This connecting method is called the “tie-rod and bolt” method [14]. The clamping load is controlled through adjusting the tightening torque applied to the nuts.

* Corresponding author.
E-mail address: cwwu@dlut.edu.cn (C.W. Wu).

0378-7753/$ – see front matter © 2009 Elsevier B.V. All rights reserved.
doi:10.1016/j.jpowsour.2009.09.038

Nomenclature

A	cross-section area (m^2)
b	width of the sealant (m)
C	design number of bolts in the stack
D_1	outside diameter of the nut (m)
D_0	inside diameter of the nut (m)
d	nominal diameter of the bolt (m)
d_1	minor diameter of the bolt (m)
d_{eq}	equivalent frictional diameter (m)
F	load (N)
k	equivalent stiffness ($N\,m^{-1}$)
M	design number of cells in the stack
n_{safe}	safety factor
P	pressure (Pa)
T	tightening torque (N m)
$Z^{thermal}$	thermal deformation (m)

Greek symbols

β	half of the thread angle in the vertical cross-section (°)
γ	number of ribs in a single flow field
δ	thread pitch (m)
ζ	coefficient of material transience from elastic to plastic
θ	frictional angle (°)
κ	in-plane gas permeability of the GDL (m^2)
μ	friction coefficient between a screw pair
ρ	contact resistivity of the GDL ($\Omega\,m^2$)
σ	stress (Pa)
φ	slope angle of the thread (°)

When tightening a bolt using a wrench, the total torque applied to the nut equals the sum of the frictional torque between the screw pair (T_1) and that between the nut and EP surface (T_2):

$$T = T_1 + T_2. \tag{1}$$

For the rectangular thread structure shown in Fig. 2, we have

$$F_1 \cos\varphi - F_2 \sin\varphi - \mu(F_1 \sin\varphi + F_2 \cos\varphi) = 0, \tag{2}$$

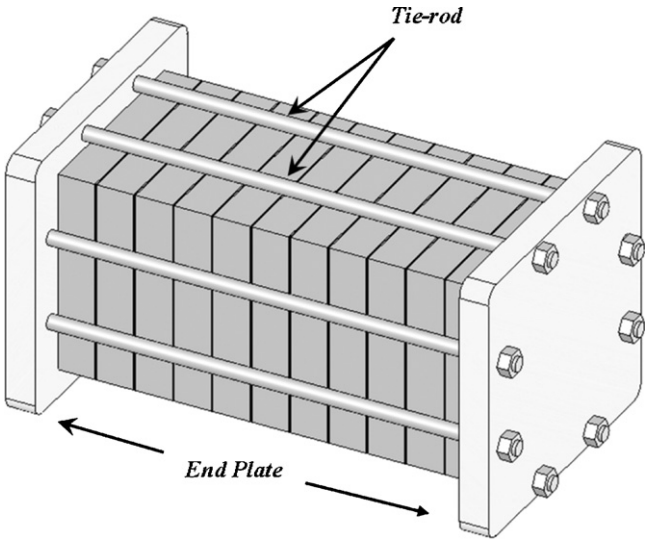

Fig. 1. Schematic diagram of the "tie-rod and bolt" method.

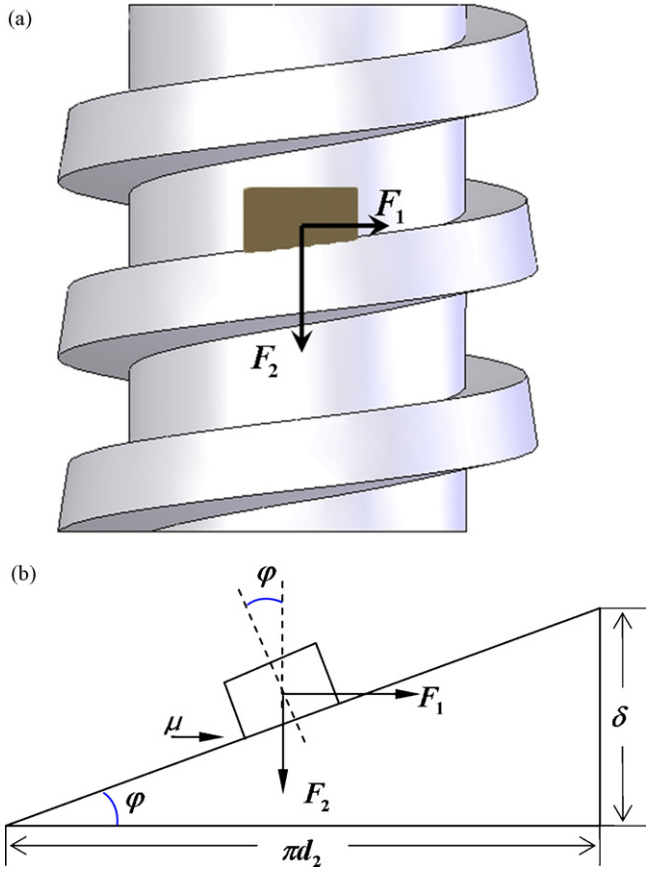

Fig. 2. Schematic diagram of the forces acting on the rectangular thread: (a) the rectangular thread and (b) the forces acting on the rectangular thread.

where φ is the slope angle of the thread, F_1 is the necessary force for spiral ascending, F_2 is the pretightening force, μ is the friction coefficient between the screw pair, and δ is the thread pitch. Letting θ be the frictional angle corresponding to μ ($\mu = \tan\theta$), Eq. (2) can be rewritten as

$$F_1 = F_2 \tan(\varphi + \theta). \tag{3}$$

Thus, the frictional torque applied to the screw pair is

$$T_1 = \frac{F_1 d}{2} = \frac{F_2 d \tan(\varphi + \theta)}{2}, \tag{4}$$

where d is the nominal diameter of the bolt.

On the other hand, the frictional torque between the nut and EP surface is

$$T_2 = \frac{\mu_n F_2}{\pi(D_1^2 - D_0^2)} \int_{D_0}^{D_1} \pi D^2 dD = \frac{\mu_n F_2 (D_1^3 - D_0^3)}{3(D_1^2 - D_0^2)}, \tag{5}$$

where D_1 is the outer diameter of the nut, D_0 is the inner diameter of the nut, and μ_n is the coefficient of the friction between the contact surfaces (see Fig. 3). Therefore, the relation between the pretension force and tightening torque is

$$T = T_1 + T_2 = F_2 \left[\frac{d \tan(\varphi + \theta)}{2} + \frac{\mu_n ({D_1}^3 - {D_0}^3)}{3({D_1}^2 - {D_0}^2)} \right]. \tag{6}$$

In general, the magnitudes of φ and θ are extremely small. In such a case, we have

$$\tan(\varphi + \theta) \approx \tan\varphi + \tan\theta. \tag{7}$$

In addition, the thread pitch can be expressed as

$$\delta = \pi d \tan\varphi. \tag{8}$$

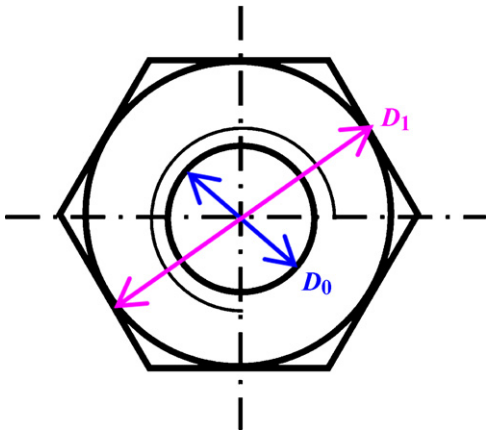

Fig. 3. Schematic diagram of the nut geometry.

Thus, Eq. (6) can be rewritten in an approximate form as

$$T \approx F_2 \left[\frac{\delta}{2\pi} + \frac{\mu d}{2} + \frac{\mu_n ({D_1}^3 - {D_0}^3)}{3({D_1}^2 - {D_0}^2)} \right]. \quad (9)$$

For the triangle thread structure, Eq. (9) should be modified as

$$T \approx F_2 \left[\frac{\delta}{2\pi} + \frac{\mu d}{2\ \cos\beta} + \frac{\mu_n (D_1^3 - D_0^3)}{3(D_1^2 - D_0^2)} \right], \quad (10)$$

where β is half of the thread angle. In the following, only triangle thread structures are adopted. In addition, a parameter called the "equivalent frictional diameter" (d_{eq}) is introduced here for equation simplification:

$$d_{eq} = \frac{\delta}{2\pi} + \frac{\mu d}{2\ \cos\beta} + \frac{\mu_n (D_1^3 - D_0^3)}{3(D_1^2 - D_0^2)}. \quad (11)$$

Therefore, Eq. (10) can be rewritten for PEMFC stacks:

$$T \approx \frac{F_{clamping} d_{eq}}{C}, \quad (12)$$

where $F_{clamping}$ is the summation of the clamping loads applied to different bolts and C is the total number of tightening bolts in the stack.

3. Stack design based on structural strength

As the voltage and power generated by a single PEMFC are rather limited, fuel cell products in engineering always comprise numerous single cells in series that form a large stack with a cyclic cell characteristic as shown in Fig. 4. Although the working principle is not different for a single cell and a stack, influences of the clamping load and thermal effects on the system performance are more complex for the stack than for the single cell [13]. In the following, we describe in detail the design procedure for a demonstration PEMFC stack structure.

A fuel cell stack generally comprises two types of structures: (a) structures used to generate power, usually residing in the internal region of the stack, and (b) structures for the sealing function, which are usually located in the external region of the stack. We refer to them as the internal-stack and external-stack respectively in the equivalent stiffness model [8]. For the internal-stack, adjusting the clamping load usually influences power-related parameters such as the permeability and interfacial resistivity of the GDL. For the external-stack, however, adjusting the clamping load mainly influences the sealing performance.

The following design description is mainly based on the structural strength. Unless noted otherwise, all the symbols used in this paper have the same meanings as those used in our previous report [8].

3.1. Relation between the tightening torque and clamping load

Washers are a type of fastener usually used with bolts and nuts. They are generally divided into flat washers and spring washers, as shown in Fig. 5. If washers, especially spring washers, need to be used in a stack assembly, the original equivalent stiffness model established in our previous report [8] may need a simple amend-

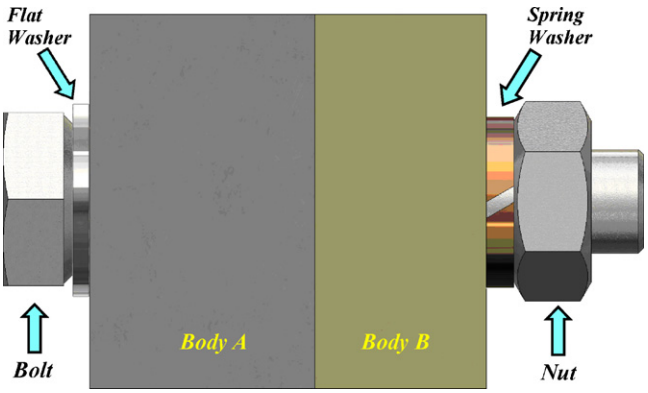

Fig. 5. Schematic diagram of the bolt connection using washers and nut.

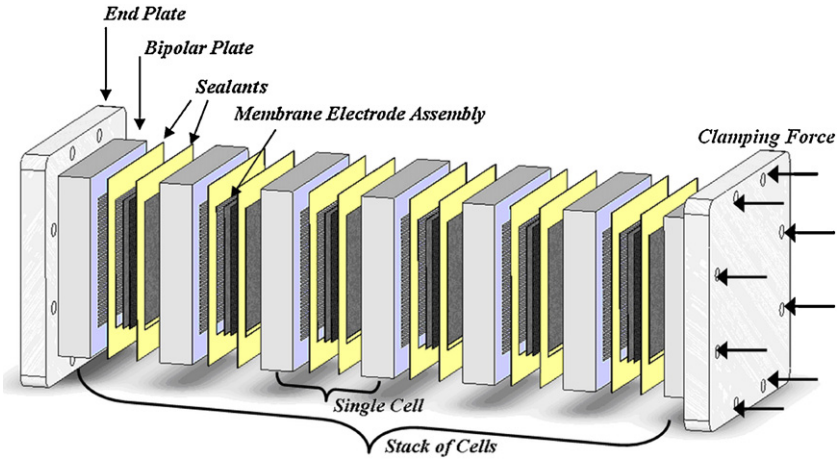

Fig. 4. Schematic diagram of the PEMFC stack hardware.

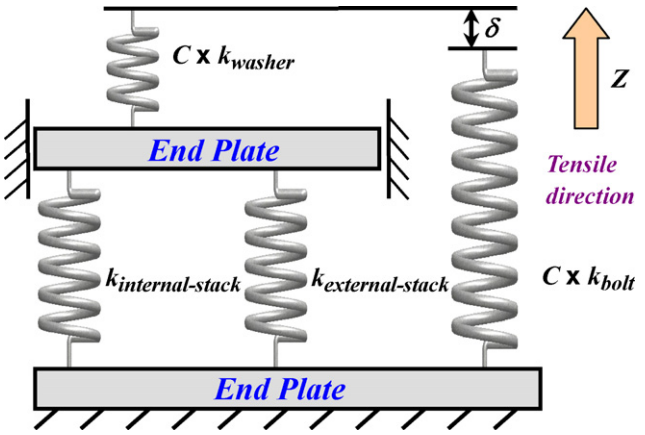

Fig. 6. Schematic diagram of the modified equivalent stiffness model when considering the washer deformation. (The spring dimension does not represent the magnitude of stiffness.)

ment, as shown in Fig. 6. Moreover, the elastic deformation of nuts is not considered in the equivalent stiffness model owing to their high stiffness and limited thickness.

According to the rigid EP assumption, the internal and external-stacks have the same deformation after applying the clamping load; that is,

$$\frac{F_{internal-stack}}{k_{internal-stack}} = \frac{F_{external-stack}}{k_{external-stack}} = \frac{F_{whole-stack}}{k_{internal-stack} + k_{external-stack}}. \tag{13}$$

From the conditions of static load equilibrium, one obtains

$$F_{whole-stack} = F_{clamping}. \tag{14}$$

The left side of Eq. (14) represents the total compression load applied to the stack, while the right side is the total tensile load applied to all bolts. Those two loads are opposite in direction, but the same in magnitude. Substituting Eqs. (14) into (13), one has

$$F_{clamping} = \frac{(k_{internal-stack} + k_{external-stack})F_{internal-stack}}{k_{internal-stack}} = \frac{(k_{internal-stack} + k_{external-stack})F_{external-stack}}{k_{external-stack}}. \tag{15}$$

Combining Eq. (12) with (15) gives relations between the tightening torque and clamping load:

$$T \approx \frac{(k_{internal-stack} + k_{external-stack})F_{internal-stack}}{Ck_{internal-stack}} d_{eq} \tag{16}$$

and

$$T \approx \frac{(k_{internal-stack} + k_{external-stack})F_{external-stack}}{Ck_{external-stack}} d_{eq}. \tag{17}$$

3.2. Clamping load design based on the strength of the external-stack

For practical PEMFCs, sealants (e.g., sealing washers or sealing rings [15]) are usually placed between BPPs to prevent the leaking of gas and coolant, the typical materials of which are Viton, ethylene–propylene–diene monomer and silicone [16]. One of the most important factors affecting the sealing performance is the mean contact pressure on the sealing surfaces. Too low a contact pressure may cause leakage, while too high a contact pressure may damage the sealants or other components. To ensure sealing performance, the mean contact pressure ($P_{sealant}$) should meet the following condition.

$$P_{sealant}^{min} \le P_{sealant} \le P_{sealant}^{max}, \tag{18}$$

where $P_{sealant}^{min}$ is the necessary mean contact pressure to prevent leakage and $P_{sealant}^{max}$ is the maximum mean contact pressure for which the sealant material does not fail. From experimental studies [17], we have the following empirical equations.

$$P_{sealant}^{min} = \frac{5.5 \times 10^6 + 3.2P_{gas}}{\sqrt{1000b}}, \tag{19}$$

$$P_{sealant}^{max} = \zeta\sigma_{sealant}^{yield}, \tag{20}$$

where P_{gas} is the gas pressure of the fuel cell, b is the width of the sealant, ζ is the transient coefficient of the sealant material from elastic to plastic deformation (roughly having a value of 3 for most polymeric materials), and $\sigma_{sealant}^{yield}$ is the yield stress of the sealant material. The range of the clamping load applied to the external-stack can then be determined using

$$\frac{(5.5 \times 10^6 + 3.2P_{gas})A_{sealant}}{\sqrt{1000b}} \le F_{external-stack} \le \zeta\sigma_{sealant}^{yield}A_{sealant}. \tag{21}$$

Therefore, the allowed range of the tightening torque applied to a single bolt on the basis of the strength requirement of the external-stack can be written as

$$T \ge \left[\frac{(5.5 \times 10^6 + 3.2P_{gas})(k_{internal-stack} + k_{external-stack})A_{sealant}d_{eq}}{\sqrt{1000b}Ck_{external-stack}}\right], \tag{22}$$

$$T \le \left[\frac{(k_{internal-stack} + k_{external-stack})\zeta\sigma_{sealant}^{yield}A_{sealant}d_{eq}}{Ck_{external-stack}}\right]. \tag{23}$$

3.3. Clamping load design based on the strength of the internal-stack

The membrane electrode assembly (MEA) plays an important role in power output. It is located in the internal-stack and can be considered a sandwich structure of "GDL + proton exchange membrane (PEM) + GDL" [8]. Since the GDL and PEM can be both highly deformed owing to either the high porosity or the low elastic modulus, the MEA deformation makes a primary contribution to the stack deformation [18]. Most of the MEA deformation is caused by the clamping load, although other factors, such as the pressures and humidities of the fuel and oxidant, the material properties, and the thickness of the sealant layer, may also affect the MEA deformation. It has been reported that failures of MEAs are mainly caused by the clamping load and thermal stress [19,20].

An electric circuit forms as soon as the BPP makes contact with the GDL during assembly. If the clamping load applied to the contact surface is not large enough, there is an unreasonably high contact resistance that produces an unexpected voltage drop in the circuit. Therefore, the minimum clamping load applied to the internal-stack should be higher than the load caused by the fuel gas pressure. However, it can share the same lower bound with the external-stack as given by Eq. (22). On the other hand, the clamping load applied to the internal-stack should not be so large that the stress in the components reaches its yield limit. As a strength design criterion, the PEM should not be susceptible to plastic deformation because of its important function [5]; i.e.,

$$F_{internal-stack} \le \gamma\sigma_{PEM}^{yield}A_{rib}, \tag{24}$$

where γ is the number of ribs on a single side of the BPP. Combining Eq. (16) with (24), the maximum allowable tightening torque

applied to a single bolt when considering the strength of the internal-stack is

$$T \le \left[\frac{(k_{internal-stack} + k_{external-stack})\gamma\sigma_{PEM}^{yield} A_{rib} d_{eq}}{Ck_{internal-stack}} \right]. \quad (25)$$

3.4. Thermal effects

As one of the design requirements is that no component gives rise to plastic deformation in any operation situation (in other words, only elastic deformations occur), the influence of the thermally induced deformation does not depend on the history of the temperature variation, but merely depends on the magnitude of the temperature variation from the assembly to the stable operating condition. When taking washers into consideration (see Fig. 6), our original equations [8] for calculating thermal effects require amending as follows:

$$F_{internal-stack} = -\frac{k_{internal-stack} F_{clamping}}{k_{internal-stack} + k_{external-stack}} + k_A[Z_{whole-stack}^{thermal} - (Z_{internal-stack}^{thermal} + Z_{washer}^{thermal})], \quad (26)$$

$$F_{external-stack} = -\frac{k_{external-stack} F_{clamping}}{k_{internal-stack} + k_{external-stack}} + k_B\left[Z_{whole-stack}^{thermal} - (Z_{external-stack}^{thermal} + Z_{washer}^{thermal})\right], \quad (27)$$

where positive values of $F_{internal\text{-}stack}$ and $F_{external\text{-}stack}$ represent tensile loads, $Z^{thermal}$ represents thermal deformation with the subscript denoting the corresponding component, and k_A and k_B are two parameters merely used for equation simplification and can be written as

$$k_A = \frac{Ck_{washer} k_{internal-stack}}{Ck_{\text{washer}} + (k_{internal-stack} + k_{external-stack})}, \quad (28)$$

$$k_B = \frac{Ck_{washer} k_{external-stack}}{Ck_{washer} + (k_{internal-stack} + k_{external-stack})}. \quad (29)$$

Strictly speaking, the magnitudes of the temperature variations of different components differ. For example, the temperature variation of the internal-stack ranges from the minimum environment temperature to the maximum operation temperature, while the temperature variation range of the external-stack and bolts may be relatively small owing to natural heat transfer. To obtain the detailed temperature distribution of the whole stack requires a numerical simulation or a temperature monitor, which is quite difficult and time consuming. However, the numerical simulation can be replaced by a reasonable assumption for the temperature distribution. One of the simplest ways is first to assume that each component has the same temperature as the corresponding region (internal-stack, external-stack and bolts) and then determine the possible temperature variations for each region. With this assumption, the equations for calculating thermal deformations are transformed as follows [8]:

$$Z_{whole-stack}^{thermal} = \frac{Ck_{bolt} Z_{bolt}^{thermal} + k_A Z_{internal-stack}^{thermal} + k_B Z_{external-stack}^{thermal} + (k_A + k_B) Z_{washer}^{thermal}}{Ck_{bolt} + k_A + k_B}, \quad (30)$$

$$Z_{external-stack}^{thermal} = (M+1) Z_{BPP-sealant}^{thermal} + M Z_{sealant}^{thermal}, \quad (31)$$

$$Z_{internal-stack}^{thermal} = (M+1) Z_{BPP-base}^{thermal} + M Z_{cell-core}^{thermal}, \quad (32)$$

$$Z_{cell-core}^{thermal} = 2(Z_{BPP-rib}^{thermal} + Z_{GDL}^{thermal}) + Z_{PEM}^{thermal}. \quad (33)$$

where *cell-core* represents the assembled component comprising *BPP-rib*, *GDL* and *PEM*, which were explained in detail in our earlier work [8].

3.5. Strength design of the clamping bolts

A clamping bolt of a PEMFC stack mainly bears axial tensile stress that increases with the tightening torque. On the basis of the mechanics of materials, the axial tensile stress in each bolt should meet the design criterion of the material strength:

$$\sigma_{bolt} = \frac{4F_{clamping}}{C\pi d_1^2} \le \frac{\sigma_{bolt}^{yield}}{n_{safe}} = [\sigma_{bolt}], \quad (34)$$

where d_1 is the minor diameter of the bolt, n_{safe} is the safety factor, and $[\sigma_{bolt}]$ is the allowable stress.

3.6. Design based on the structural strength

In the following, a design demonstration is given for the PEMFC stack consisting of multiple single cells as described in the work by Bograchev et al. [5] (see Fig. 7). The design numbers of cells are 5, 10, 20, 30, 40 and 50. The required material properties and operation parameters for this demonstration stack are listed in Table 1. All fasteners (bolts, nuts and washers) are initially chosen as standard series M8 fasteners. Thermal deformations of the washers are neglected owing to their relative small thickness.

First, the equivalent stiffness of the internal- and external-stacks with different numbers of cells is calculated and shown in Fig. 8. The figure shows that for the studied PEMFC stacks, the equivalent stiffness of the external-stack is always greater than that of the internal-stack, while both decrease nonlinearly as the design number of cells increases.

As the operating ambient temperature changes frequently during the use of the PEMFC stack, the temperature range of each component in the stack also varies frequently. As modern PEMFC

Table 1
Material properties and operation parameters of the stack hardware.

Description	Value	Source
Material property		
PEM (Nafion®)		
Young's modulus (MPa)	190	[21]
Coefficient of linear expansion (K^{-1})	90×10^{-6}	[22]
GDL (carbon paper)		
Young's modulus (GPa)	10	[21]
Coefficient of linear expansion (K^{-1})	7.9×10^{-6}	[22]
Bipolar plate (graphite)		
Young's modulus (GPa)	10	[21]
Coefficient of linear expansion (K^{-1})	7.9×10^{-6}	[22]
Sealant (VMQ)		
Young's modulus (MPa)	5500	[4]
Coefficient of linear expansion (K^{-1})	77×10^{-6}	[22]
Clamping bolt (steel)		
Young's modulus (GPa)	209	[23]
Coefficient of linear expansion (K^{-1})	13×10^{-6}	[22]
Washer (aluminum bronze)		
Young's modulus (GPa)	110	[23]
Operation parameters		
Gas temperature (K)	353	[24]
Gas pressure—anode (MPa)	0.15	[24]
Gas pressure—cathode (MPa)	0.15	[24]
Assembly temperature (K)	293	Assumed
Operating temperature (K)	253–353	Assumed
Inlet relative humidity—anode	100%	[24]
Inlet relative humidity—cathode	100%	[24]

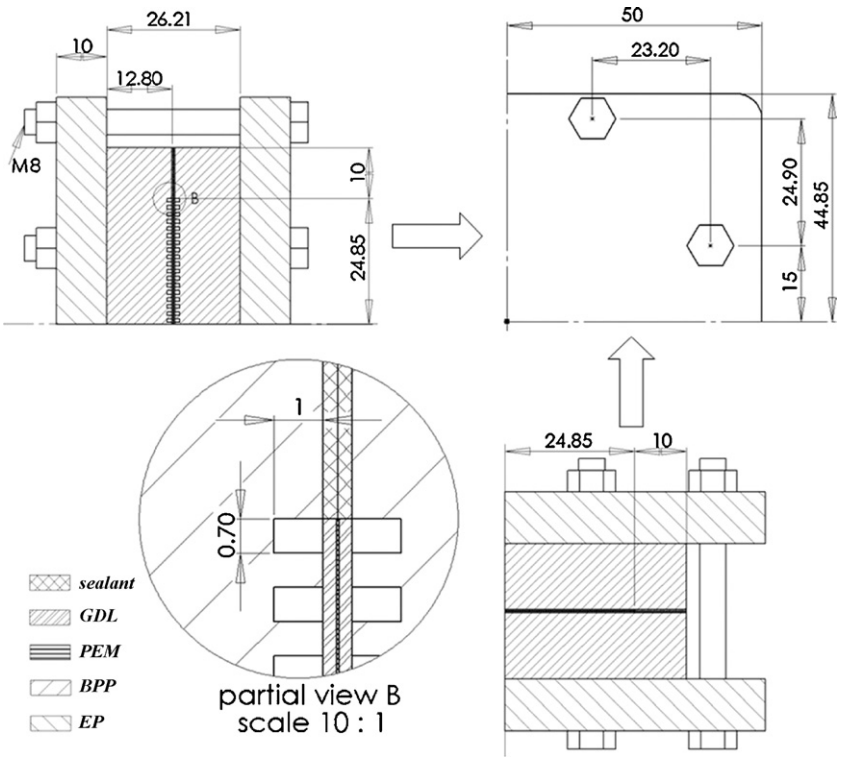

Fig. 7. Dimensions of the single cell structure of the demonstration stacks. (The washers are not drawn in this figure.)

stacks usually operate at temperatures below 353 K [25], the temperature of the MEA may range from a low ambient temperature (for example 233 K in winter) to 353 K (the working state), whereas the bolt temperature may range from the ambient temperature to a temperature higher than the ambient temperature but lower than the working temperature of the MEA. Table 1 lists some possible temperature parameters, while Table 2 presents the five possible cases for the stack components. The first and second cases correspond to a low ambient temperature and high ambient temperature respectively (stack in a rest state); case 3 assumes that the stack is working at a low ambient temperature; case 4 assumes that the stack is working at room temperature; while case 5 assumes that the stack is working at a high temperature (a limit case). All the studied stacks were assembled at room temperature (293 K).

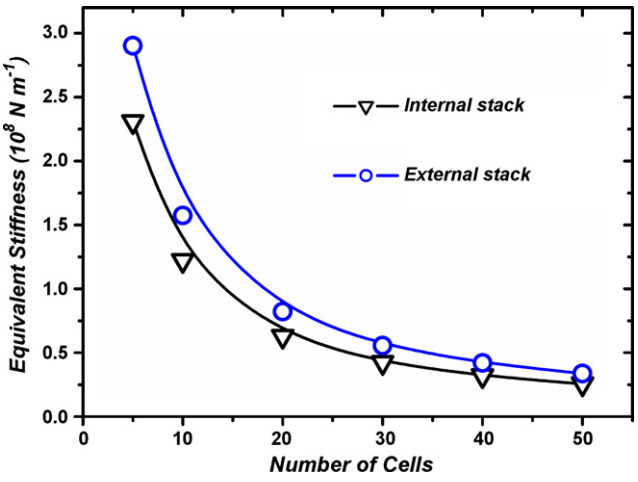

Fig. 8. Variation in the equivalent stiffness with the design number of cells.

Using the parameters given above, the thermal effects can be calculated using Eqs. (26)–(33), where the magnitude of the temperature variation for any component equals the difference between its corresponding working temperature (or the rest state if not working) and assembly temperature. Fig. 9 shows that all the thermal loads vary nonlinearly with the design number of cells. Moreover, both the internal- and external-stacks are subjected to compression loads while the bolts are subjected to tensile loads in cases 1, 3 and 4, whereas the opposite is true in the other two cases.

In general, the PEMFC stack should be designed to meet the requirements of the structural strength for all possible conditions; i.e., the five cases listed in Table 2. Taking a specified case for example, once the design number of cells has been fixed, the corresponding lower bound of the tightening torque is given by Eq. (22), while the upper bound is the minimum of tightening torques obtained from Eqs. (23) and (25). Considering all five cases mentioned above, the allowable range of the tightening torque for the studied stack is shown in Fig. 10. That is, if the tightening torque is designed within the allowable range, no damage will occur.

The design is not yet finished since the strength of the clamping bolts has not been checked. Normally, only the upper bound of the tightening torque needs to be calculated using Eq. (34) for the bolt

Table 2
Assumed temperature variations in four cases.

	Case 1	Case 2	Case 3	Case 4	Case 5
Assembly temperature (K)	293	293	293	293	293
Ambient temperature (K)	233	313	233	293	353
Assumed working temperature[a] (K)					
Internal-stack	233	313	353	353	353
External-stack	233	313	313	333	353
Bolt	233	313	298	313	353

[a] Working temperature includes the temperature when the stack is at rest in the non-operating case.

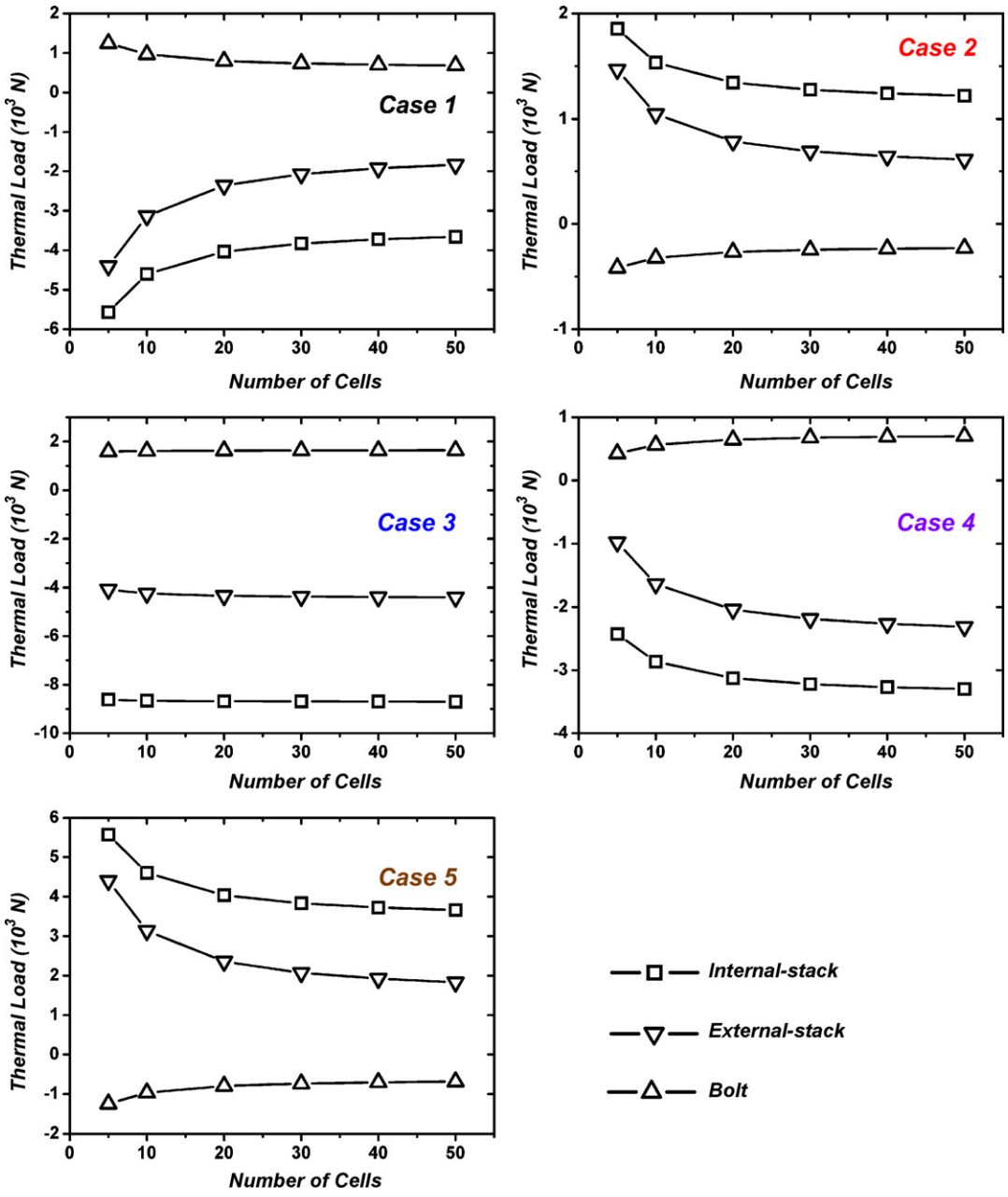

Fig. 9. Calculated thermal loads for the cases given in Table 2.

strength design. For the studied stacks, it is found that the tightening torque is located in the allowable area (see Fig. 10) and the calculated safety factor for the bolt strength is 2.8 when the bolt diameter is designed as 8 mm (M8).

4. Design based on the stack performance

The optimal clamping load can be chosen in the area of the allowable range after the strength-based design. It is an interesting and important topic how to design the optimal clamping load via controlling the tightening torque for a special PEMFC stack. Strictly speaking, searching for the optimal clamping load is a multi-objective optimization problem, which is a difficult topic in the computational mechanics since the clamping load dramatically affects the stack performance in a complex manner. One needs first to accurately know the relations between the performance parameters and the clamping load. However, on the basis of the equivalent stiffness model, we introduce here a method for obtaining the optimal clamping load for a given PEMFC stack.

4.1. Variation in the interfacial resistance between the GDL and BPP with tightening torque

The contact resistance of a pair of solid surfaces is governed by the multiscale surface topography and the surface physical properties. When two solid surfaces are in contact under a small compression force, only the tips of the surface asperities come into contact and thus the real contact area is very small [26]. In such a case, the interfacial resistance is very high. The real contact area increases with the compression pressure, while the Ohmic resistance decreases. For the fuel cells, the clamping load should be large enough to give an acceptably small overall Ohmic resistance.

Several experiment datasets for the interfacial contact resistance of a single fuel cell and the total resistance including the

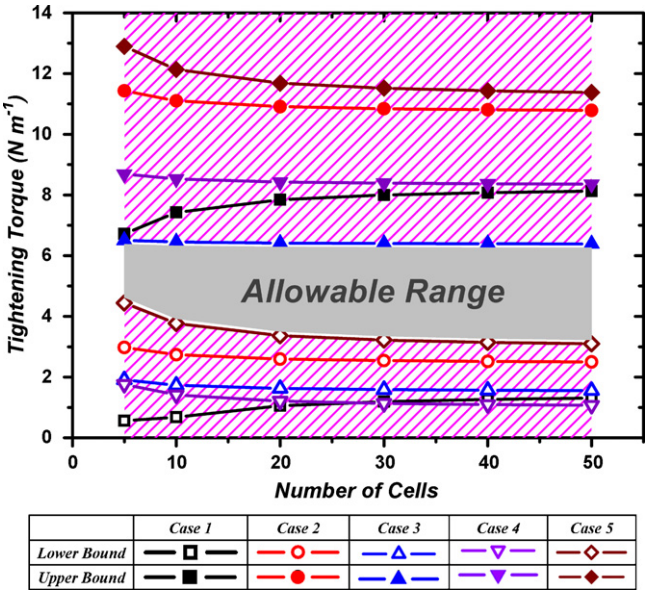

Fig. 10. The allowable range of the tightening torque applied to a single nut when considering all five cases listed in Table 2. (Hatched areas are those for which a tightening torque is not allowed.)

bulk resistance are available in the literature. Mishra et al. [27] measured the total resistance and the interfacial contact resistance between different GDLs and graphite BPPs. They proposed a fractal asperity-based model to predict the interfacial contact resistance as a function of pressure, material properties and surface geometry. Wang et al. [28] reported the interfacial contact resistances between a Toray carbon paper (Electro-Chem Inc.) and four types of stainless steel BPPs. Ihonen et al. [29] conducted in situ measurements of the interfacial contact resistance as a function of time, clamping pressure, gas pressure and current density. From the experimental data given in the work by Mishra et al. [27], Zhou et al. [1] established a mathematical model for the interfacial contact resistivity between a GDL and BPP:

$$\rho = B_1 \left(\frac{B_2}{P_{GDL}} \right)^{B_3}, \tag{35}$$

where ρ is the interfacial contact resistivity, B_1, B_2 and B_3 are coefficients determined by experiments, and P_{GDL} is the contact pressure at the GDL, which can be calculated using

$$P_{GDL} \approx \frac{F_{internal-stack} - P_{gas} A_{GDL}}{\gamma A_{rib}}. \tag{36}$$

Therefore, the interfacial contact resistivity can be determined by combining Eqs. (16), (35) and (36):

$$\rho \approx B_1 \left[\frac{B_2 \gamma A_{rib} d_{eq} (k_{internal-stack} + k_{external-stack})}{TCk_{internal-stack} - P_{gas} A_{GDL} d_{eq} (k_{internal-stack} + k_{external-stack})} \right]^{B_3}. \tag{37}$$

4.2. Variation in the GDL's in-plane permeability with tightening torque

Permeability is another important performance parameter of the GDL that depends on the clamping load. In a PEMFC, liquid water is produced during operation and exchanges at the interface of the catalyst layer and microporous layer. During the water transportation, the capillary pressure gradient must overcome the negative pressure gradient of the gas phase. Therefore, a low permeability leads to a high gas pressure gradient and high liquid water saturation, which in turn reduces the stack performance [30]. Chang et al. [24] measured the effects of the clamping load on the performance of the PEMFC and provided an empirical relation between

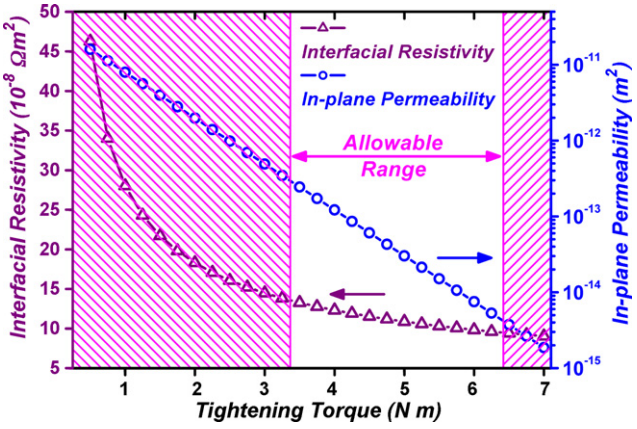

Fig. 11. Variation of the GDL interfacial resistivity and permeability with the tightening torque. (Hatched areas are those for which a tightening torque is not allowed; the design number of cells is 20.)

the in-plane permeability κ and the clamping load:

$$\kappa = \kappa_0 \exp[-8.23 \times 10^3 P_{GDL}], \tag{38}$$

where κ_0 is the initial in-plane permeability. In the present paper, Eqs. (16), (36) and (38) are combined to obtain the relation between the GDL permeability and tightening torque:

$$\kappa = \kappa_0 \exp \left\{ \frac{-8.23 \times 10^3 [TCk_{internal-stack} - P_{gas} A_{GDL} d_{eq} (k_{internal-stack} + k_{external-stack})]}{\gamma A_{rib} d_{eq} (k_{internal-stack} + k_{external-stack})} \right\}. \tag{39}$$

Taking a stack consisting of 20 cells as an example, variations in the GDL interfacial resistivity and permeability with the tightening torque are shown in Fig. 11. It is shown that both of the parameters decrease nonlinearly with an increasing clamping load. However, they are contradictory factors influencing the stack performance. Thus, the optimal tightening torque should be chosen after balancing all possible effects. For the present design example, as the interfacial resistivity changes only slightly within the allowable range of the tightening torque, the optimal tightening torque can be determined mainly on the basis of GDL permeability; i.e., the tightening torque should be applied as close to the left side of the allowable region as possible.

5. Discussions

5.1. Considering the equivalent stiffness of nuts

In general, the effects of nuts on the equivalent stiffness model can be ignored for several reasons: (a) compared with the clamping bolts, especially in a large PEMFC stack, deformations of the nuts are rather limited, (b) unlike spring washers, the equivalent stiffness of the nut is very low, and (c) the clamping force mainly acts on the first few threads (close to the EP) [31]. However, when the stiffness of the nut has to be considered, we can simply extend the effective length of the clamping bolt by a suitable percentage of the nut thickness.

5.2. How thermal stress affects the optimal clamping load

If all thermal effects are neglected, the design process is simple since no working condition has to be considered. However, the thermal calculation cannot be skipped in the practical design owing to its great effect on the design results. Fig. 12 compares the design that considers the thermal effect and the design that does not.

It is found that the allowable range of the tightening torque when considering thermal effects is much smaller than that when

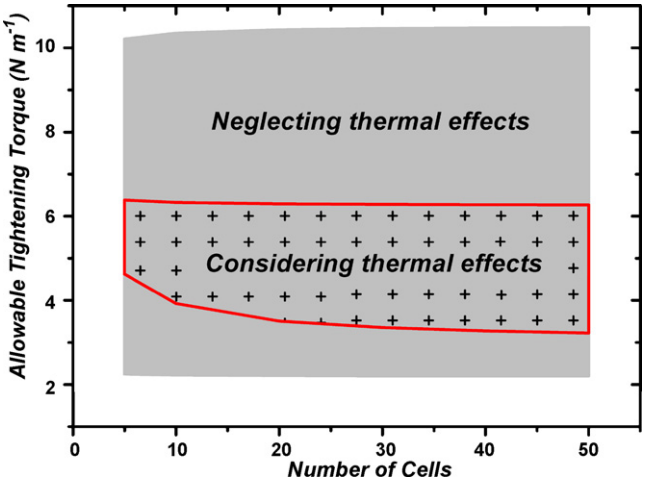

Fig. 12. Comparison of the design results with and without consideration of thermal effects.

neglecting thermal effects. In other words, thermal loads (stresses) are so large that they may damage the stack components if the clamping load is not optimized by considering the thermal effect.

5.3. The role of spring washer stiffness

Besides preventing the nuts from loosening, the spring washers (hereafter simply referred to as washers) have other useful functions. One function is the adjustment of the thermal loads inside the stacks through the design of a suitable equivalent stiffness for the washer.

Taking the stack consisting of 20 cells in case 4 as an example, the effects of the equivalent stiffness of washers on the thermal loads are shown in Fig. 13. The figure shows that the absolute values of the thermal loads in both the internal- and external-stacks decrease nonlinearly with an increase in the equivalent stiffness of the spring washer. If the stiffness of the washer is designed to be low enough (less than 2.5×10^8 N m^{-1}), the effects of the thermal loads can be effectively reduced. However, if the stiffness exceeds 5×10^8 N m^{-1}, the washer has almost no effect on the thermal loads acting on the bolts, internal-stack and external-stack.

Although low stiffness of the washer is helpful in reducing the thermal stress in the stack structure, an unreasonably low stiffness of the washer may also cause the stiffness of the whole stack system to decrease to an unacceptable level and thus may reduce the vibration stability of the stack system. Therefore, similar to the case for the design of the optimal tightening torque, the optimal equivalent stiffness of the washers has to be determined by considering all the practical requirements of the stack system.

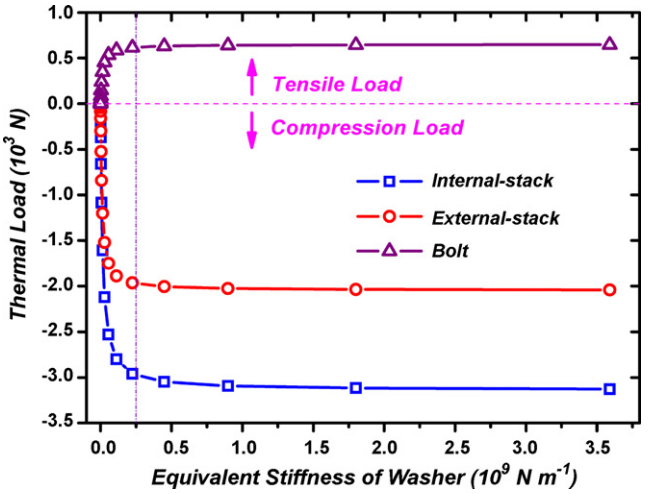

Fig. 13. Effects of the equivalent stiffness of the washer on the thermal loads (case 4; the design number of cells is 20).

6. Conclusions

In the present paper, a complete design example of a large PEMFC stack was introduced to explain step by step how to design the optimal tightening torque using the equivalent stiffness model proposed by the present authors in our previous work [8]. The design considers the stack structure strength, stack performance and thermal effects. It was shown that the equivalent stiffness of the internal-stack and that of the external-stack decrease with an increasing number of cells in the stack in a nonlinear manner and that thermal effects cannot be ignored in the structure design. Moreover, how to obtain the optimal clamping load for a given PEMFC stack was explained according to the contact resistance and permeability of the GDL, and in a practical design, the optimal tightening torque can be determined after balancing all possible effects. Finally, the effects of the equivalent stiffness of the spring washer on the structure stress in the stack were discussed. The basic design method described in the present paper can be used for any PEM stack design and may be helpful for other fuel cell stack designs.

Acknowledgements

This work was supported by the National Natural Science Foundation of China (10672035, 10721062, 90816025) and the "863" Project (2007AA04Z405).

References

[1] P. Zhou, C.W. Wu, G.J. Ma, J. Power Sources 159 (2006) 1115–1122.
[2] P. Zhou, C.W. Wu, G.J. Ma, J. Power Sources 163 (2007) 874–881.
[3] P. Zhou, C.W. Wu, J. Power Sources 170 (2007) 93–100.
[4] S.J. Lee, C.D. Hsu, C.H. Huang, J. Power Sources 145 (2005) 353–361.
[5] D. Bograchev, M. Gueguen, J.C. Grandidier, S. Martemianov, J. Power Sources 180 (2008) 393–401.
[6] X.M. Lai, D.A. Liu, L.F. Peng, J. Ni, J. Power Sources 182 (2008) 153–159.
[7] Z.Y. Su, C.T. Liu, H.P. Chang, C.H. Li, K.J. Huang, P.C. Sui, J. Power Sources 183 (2008) 182–192.
[8] P. Lin, P. Zhou, C.W. Wu, J. Power Sources 194 (2009) 381–390.
[9] D.H. Ahmed, H.J. Sung, J. Bae, Int. J. Hydrogen Energy 33 (2008) 3786–3800.
[10] A. Bazylak, D. Sinton, Z.S. Liu, N. Djilali, J. Power Sources 163 (2007) 784–792.
[11] D. Liu, X. Lai, J. Ni, L. Peng, S. Lan, Z. Lin, J. Power Sources 172 (2007) 760–767.
[12] S. Karvonen, T. Hottinen, J. Ihonen, H. Uusalo, J. Fuel Cell Sci. Technol. 5 (2008) 041009.
[13] M. Mikkola, T. Tingelöf, J.K. Ihonen, J. Power Sources 193 (2009) 269–275.
[14] J.S. Kim, J.B. Park, Y.M. Kim, S.H. Ahn, H.Y. Sun, K.H. Kim, T.W. Song, Int. J. Precis. Eng. Manuf. 9 (2008) 39–46.
[15] J.F. Wu, X.Z. Yuan, J.J. Martin, H.J. Wang, J.J. Zhang, J. Shen, S.H. Wu, W. Merida, J. Power Sources 184 (2008) 104–119.
[16] M. Schulze, T. Knöri, A. Schneider, E. Gülzow, J. Power Sources 127 (2004) 222–229.
[17] N.T. Romanenko, Y.F. Kulikov, Cryogenic Valves and Fittings, Mashinostrojenie, Moscow, 1976 (in Russian).
[18] W.K. Lee, C.H. Ho, J.W. Zee, M. Murthy, J. Power Sources 84 (1999) 45–51.
[19] M. Fowler, R.F. Mann, J.C. Amphlett, B.A. Peppley, P.R. Roberge, in: W. Vielstich, H.A. Gasteiger, A. Lamm (Eds.), Handbook of Fuel Cells: Fundamentals, Technology and Applications, vol. 3, John Wiley & Sons Ltd., 2003, pp. 663–677.
[20] J.F. Wu, X.Z. Yuan, J.J. Martin, H.J. Wang, X.T. Bi, P.C. Pei, H.Y. Huang, Proceedings of Hydrogen & Fuel Cell 2007, Vancouver, BC, Canada, May, 2007, pp. 448–458.
[21] A. Kusoglu, A.M. Karlsson, M.H. Santare, S. Cleghorn, W.B. Johnson, J. Power Sources 161 (2006) 987–996.
[22] http://www.engineeringtoolbox.com/linear-expansion-coefficients-d_95.html.
[23] Marc2007r1 Volume E: Demonstration Problems, MSC software, 2007.
[24] W.R. Chang, J.J. Hwang, F.B. Weng, S.H. Chan, J. Power Sources 166 (2007) 149–154.
[25] F.A. de Bruijn, V.A.T. Dam, G.J.M. Janssen, Fuel Cells 8 (2008) 3–22.
[26] J.B.P. Williamson, Proceedings of 4th International Conference on Electrical Contact Phenomena, Swansea, 1968, pp. 30–34.

[27] V. Mishra, F. Yang, R. Pitchumani, ASME J. Fuel Cell Sci. Technol. 1 (2004) 2–9.
[28] H.L. Wang, M.A. Sweikart, J.A. Turner, J. Power Sources 115 (2003) 243–251.
[29] J. Ihonen, F. Jaouen, et al., Electrochim. Acta 46 (2001) 2899–2911.
[30] L. Cindrella, A.M. Kannan, J.F. Lin, K. Saminathan, Y. Ho, C.W. Lin, J. Wertz, J. Power Sources, doi:10.1016/j.jpowsour.2009.04.005.
[31] J.W. Hobbs, E.A. Patterson, R.L. Burguete, P.F. Heyes, Proceedings of 4th International Congress on Experimental Mechanics, 2000, pp. 359–362.